# SUPPLEMENTAL MATERIALS

ASCE *Journal of Geotechnical and Geoenvironmental Engineering*

# A Framework for Assessing the Bearing Capacity of Sandy Coastal Soils from Remotely Sensed Moisture Contents

Julie Paprocki, Nina Stark, and Heidi Wadman

**DOI:** 10.1061/JGGEFK.GTENG-11339



www.ascelibrary.org

**PFFP Processing**

The portable free fall penetrometer (PFFP) *blueDrop* records accelerations up to ±250g, is 63.1 cm in length, 8.75 cm in diameter, and weighs ~7.7 kg when using the conical tip (Stark et al. 2014), which is used in the current study. The PFFP was deployed ~1 m above the sand bed and allowed to free fall until impacting the sand bed. Upon impact, the penetration velocity and depth are determined using first and second integration, respectively, of the deceleration profile. The sediment resistance force, $F_s$, can be calculated using the deceleration, $dec$, and the penetrometer mass in air, $m$:

$$F_s = m * dec \quad \text{(S1)}$$

An example of a deceleration profile is shown in Figure S1.

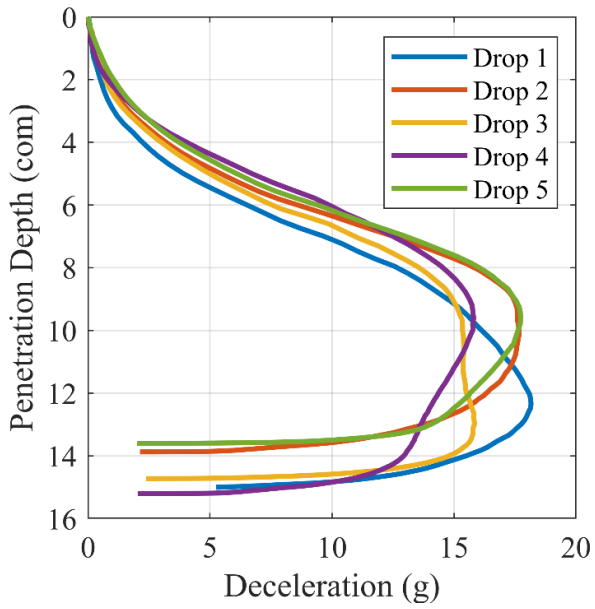


Figure S1. Deceleration profiles recorded on 07 December 2020 at station A2 in the subaerial zone. Deployments are spaced ~1 m apart to avoid effects of previous deployments.

Next, the cone area $A$ and $F_s$ is used to calculate the dynamic bearing capacity, $q_{dyn}$, of the sand:

$$q_{dyn} = \frac{F_s}{A} \quad \text{(S2)}$$

Since the shear strength of soils is dependent on the shearing rate and the penetrometer impacts at

high velocities, $q_{dyn}$ needs to be corrected to determine an equivalent static resistance, or quasi-static bearing capacity (*qsbc*). To account for these effects, $q_{dyn}$ is divided by a strain rate correction factor, $f_{sr}$ to find *qsbc*. For sandy soils, the logarithmic function is commonly used to address strain rate effects (Stark et al. 2009, 2012; Stephan et al. 2015; Stoll et al. 2007):

$$f_{sr} = 1 + K * log_{10}\left(\frac{v_{dyn}}{v_{ref}}\right) \quad \text{(S3)}$$

where $v_{dyn}$ is the dynamic penetration velocity, $v_{ref}$ is a reference penetration velocity (typically 0.02 m/s based on the standard velocity for cone penetration testing from ASTM D5778 (ASTM 2014), and $K$ is a dimensionless empirical coefficient. This parameter typically ranges between 1.0-1.5 for submerged sandy materials (Lucking et al. 2017; Stark et al. 2009, 2012, 2017; Stephan et al. 2015; Stoll et al. 2007).

**Estimating moisture content from satellite-based optical images**

Paprocki et al. (2022) proposed a framework to estimate the gravimetric moisture content from the near infrared (NIR) band of multispectral images using both field and laboratory calibrated constants for the model proposed by (Muller and Décamps 2001). Within this framework, images are first corrected to the reflectance, $\rho$, using the process outlined by (Kuester 2016). Next, the field-derived parameters for dry reflectance $\rho_{dry}$ ($\mu_{\rho_{dry}}$ = 0.2839, $\sigma_{\rho_{dry}}$ = 0.0087) and the model fitting parameter $c$ ($\mu_c$ = 0.0366) were used to estimate of the moisture content using Equation (S4):

$$\mu_{mc} = \frac{\ln\left(\frac{\rho}{\rho_{dry}}\right)}{-c} \quad \text{(S4)}$$

To estimate the standard deviation, a First Order, Second Moment (FOSM) analysis was performed on Equation (S4), resulting in Equation (S5):

(S5) $$\sigma_{mc}^2 = \left(\frac{1}{c\mu_{\rho_{dry}}}\right)^2 * \sigma_{\rho_{dry}}^2$$

where $\sigma_{mc}^2$ is the variance of the moisture content. The standard deviation of moisture content is found by taking the square root of Equation (S5). For each point, the value of $\rho$ at that pixel was averaged with the $\rho$ of eight adjacent pixels to estimate moisture content.

**Estimating moisture content from the satellite-based SAR image**

For synthetic aperture radar (SAR) images, volumetric moisture contents were estimated using the models presented in Paprocki (2022a). Images were first calibrated to the horizontally polarized backscatter coefficient, $\sigma_{HH}^0$, and the average of nine adjacent pixels was found. Next, the beach slope, normalized backscatter (taken as the ratio $\sigma_{HH}^0/\theta$), $\sigma_{HH}^0$ in decibels, and the roughness category (which is classification of $\sigma_{HH}^0$ with regards to the transmitted wavelength and $\theta$) were used to estimate the root mean square (or RMS) height of the pixel for that given roughness category. Beach slopes were obtained from the digital elevation model (DEM) collected ~4 mins following SAR image collection from the Rigel Z390 terrestrial laser scanner mounted to the research pier at the USACE-FRF (Brodie et al. 2017) The moisture content for the RMS height of that roughness category was then calculated using the model presented by (Oh 2004); this process was repeated for all roughness categories. Finally, the moisture content was estimated using Equation (S6):

(S6) $$\mu_{mc} = \sum_{i=1}^{i=3} P(Category_i) \cdot mc_i$$

where $P(Category_i)$ is the probability of the $i^{th}$ roughness category and $mc_i$ is the estimated moisture content of the $i^{th}$ roughness category. If the estimated moisture content is lower than [-

$6.286/\ln(\theta/90)]^{-1.538}$, it was set to this value.

Using the trends observed from field measurements, the standard deviation of the moisture content can be calculated using the relationship proposed by (Famiglietti et al. 1998)

(S7) $$\sigma_{mc} = a \cdot \mu_{mc} \cdot \exp(-b \cdot \mu_{mc})$$

where $a$ and $b$ are model fit parameters founding using sum of square error regression.

From field measurements, $a$ = 0.548 and $b$ = 0.055.

**Bearing Capacity Factors**

For this study, the bearing capacity factors from (Vesić 1973) were used for the sensitivity analysis and to estimate the best path for driving on the beach, assuming that the contact area of the tire is a rectangle:

(S8) $$N_q = tan^2\left(\frac{\pi}{4} + \frac{\phi}{2}\right) \cdot \exp(\pi \cdot tan\phi)$$

(S9) $$N_c = \left(N_q - 1\right) \cdot cot\phi$$

(S10) $$N_\gamma = 2 \cdot \left(N_q + 1\right) \cdot tan\phi$$

Additionally, the shape factors from (De Beer 1970) were used:

(S11) $$\xi_c = 1 + \left(\frac{B}{L} \cdot \frac{N_q}{N_c}\right)$$

(S12) $$\xi_q = 1 + \left(\frac{B}{L}\right) \cdot tan\phi$$

(S13) $$\xi_\gamma = 1 - 0.4 \cdot \left(\frac{B}{L}\right)$$

Finally, the load inclination factors from (Meyerhof 1963) were used to estimate the probability of failure for vehicles:

(S14) $$i_c = i_q = \left(1 - \frac{2 \cdot \alpha}{\pi}\right)^2$$

(S15) $$i_\gamma = \left(1 - \frac{\alpha}{\phi}\right)^2$$

**Summary of laboratory testing on Duck, NC sand**

Table S1 presents the results of the testing performed on the sediment samples collected in Duck, North Carolina over the duration of the study. In total, 127 of the 128 samples collected were analyzed for the grain size and unit weight; sample A1 on 07 September 2020 was excluded from analysis. For full details related to sediment testing, please refer to the data repository (Paprocki 2022b).

Table S1. Summary of sand samples from Duck, NC

| Date | Station | $d_{60}$ (mm) | $d_{50}$ (mm) | $d_{30}$ (mm) | $d_{10}$ (mm) | $C_u$ | $C_c$ | $w_c$ (%) | $\gamma$ (kN/m$^3$) | Void Ratio, $e$ | $M_v$ (%) | Wentworth Classification | USCS Classification | Heavy Minerals? |
|---|---|---|---|---|---|---|---|---|---|---|---|---|---|---|
| 9/7/2020 PM | A4 | 0.281 | 0.251 | 0.201 | 0.160 | 1.76 | 0.89 | 5.4 | 17.0 | 0.65 | 20.9 | medium | SP | Yes |
| | A7 | 0.291 | 0.259 | 0.205 | 0.162 | 1.79 | 0.89 | 20.4 | 19.9 | 0.61 | 27.0 | medium | SP | No |
| | B3 | 0.294 | 0.260 | 0.203 | 0.158 | 1.86 | 0.88 | 0.6 | 16.8 | 0.59 | 4.0 | medium | SP | No |
| 9/8/2020 AM | A1 | 0.289 | 0.256 | 0.201 | 0.158 | 1.83 | 0.89 | 0.6 | 16.5 | 0.62 | 2.6 | medium | SP | No |
| | A4 | 0.265 | 0.234 | 0.183 | 0.125 | 2.12 | 1.01 | 1.9 | 16.0 | 0.69 | 21.2 | fine | SP | Yes |
| | A7 | 0.290 | 0.259 | 0.206 | 0.164 | 1.76 | 0.89 | 6.1 | 14.7 | 0.92 | 11.2 | medium | SP | No |
| | B5 | 0.276 | 0.247 | 0.199 | 0.160 | 1.73 | 0.90 | 4.0 | 14.5 | 0.91 | 5.9 | fine | SP | No |
| 9/8/2020 PM | A1 | 0.291 | 0.259 | 0.205 | 0.162 | 1.79 | 0.89 | 1.2 | 16.5 | 0.63 | 6.6 | medium | SP | No |
| | A4 | 0.275 | 0.245 | 0.195 | 0.155 | 1.77 | 0.89 | 3.6 | 16.1 | 0.71 | 16.8 | fine | SP | Yes |
| | A7 | 0.291 | 0.259 | 0.205 | 0.162 | 1.79 | 0.89 | 22.1 | 19.4 | 0.67 | 31.2 | medium | SP | No |
| | C5 | 0.280 | 0.251 | 0.201 | 0.161 | 1.73 | 0.90 | 5.6 | 14.6 | 0.92 | 6.0 | medium | SP | No |
| 9/9/2020 AM | A1 | 0.276 | 0.249 | 0.201 | 0.163 | 1.69 | 0.90 | 1.9 | 15.5 | 0.75 | 4.3 | fine | SP | No |
| | A4 | 0.275 | 0.246 | 0.196 | 0.157 | 1.76 | 0.89 | 6.00 | 16.0 | 0.76 | 16.3 | fine | SP | Yes |
| | A7 | 0.279 | 0.250 | 0.200 | 0.161 | 1.74 | 0.90 | 17.8 | 17.3 | 0.81 | 23.3 | medium | SP | No |
| | C5 | 0.278 | 0.249 | 0.201 | 0.161 | 1.72 | 0.90 | 3.6 | 14.2 | 0.94 | 3.9 | fine | SP | No |
| 9/10/2020 PM | A1 | 0.390 | 0.330 | 0.236 | 0.168 | 2.32 | 0.85 | 5.9 | 16.8 | 0.68 | 5.0 | medium | SP | No |
| | A4 | 0.276 | 0.243 | 0.188 | 0.135 | 2.05 | 0.95 | 5.7 | 16.2 | 0.73 | 10.0 | fine | SP | No |
| | A7 | 0.299 | 0.266 | 0.209 | 0.165 | 1.82 | 0.89 | 22.0 | 19.6 | 0.65 | 28.5 | medium | SP | No |
| | B4 | 0.264 | 0.235 | 0.186 | 0.138 | 1.92 | 0.95 | 6.50 | 17.6 | 0.61 | 18.8 | fine | SP | Yes |
| 9/11/2020 AM | A1 | 0.628 | 0.387 | 0.253 | 0.166 | 3.79 | 0.62 | 4.3 | 16.5 | 0.68 | 2.6 | medium | SP | No |
| | A4 | 0.256 | 0.226 | 0.176 | 0.112 | 2.28 | 1.07 | 5.7 | 15.7 | 0.79 | 8.9 | fine | SP | No |
| | A7 | 0.278 | 0.249 | 0.199 | 0.160 | 1.74 | 0.90 | 16.7 | 16.7 | 0.86 | 21.8 | fine | SP | No |
| 9/11/2020 PM | A1 | 0.799 | 0.494 | 0.283 | 0.177 | 4.53 | 0.57 | 4.5 | 16.6 | 0.67 | 3.1 | medium | SP | No |
| | A4 | 0.276 | 0.245 | 0.192 | 0.150 | 1.84 | 0.89 | 3.4 | 16.0 | 0.72 | 7.5 | fine | SP | No |
| | A6 | 0.281 | 0.252 | 0.204 | 0.165 | 1.71 | 0.90 | | N/A | | | Medium | SP | No |
| | A7 | 0.310 | 0.273 | 0.213 | 0.165 | 1.87 | 0.88 | 21.3 | 19.7 | 0.64 | 34.2 | medium | SP | No |
| 10/5/2020 PM | A1 | 0.276 | 0.248 | 0.200 | 0.162 | 1.70 | 0.90 | 3.5 | 15.4 | 0.79 | 3.0 | fine | SP | No |
| | A4 | 0.293 | 0.261 | 0.207 | 0.164 | 1.79 | 0.89 | 4.8 | 14.7 | 0.89 | 12.2 | medium | SP | No |

| Date | Station | $d_{60}$ (mm) | $d_{50}$ (mm) | $d_{30}$ (mm) | $d_{10}$ (mm) | $C_u$ | $C_c$ | $w_c$ (%) | $\gamma$ (kN/m$^3$) | Void Ratio, $e$ | $M_v$ (%) | Wentworth Classification | USCS Classification | Heavy Minerals? |
|---|---|---|---|---|---|---|---|---|---|---|---|---|---|---|
| 10/7/2020 PM | A1 | 0.323 | 0.283 | 0.217 | 0.166 | 1.95 | 0.88 | 2.9 | 16.5 | 0.66 | 0.9 | medium | SP | No |
| | A4 | 0.287 | 0.256 | 0.204 | 0.162 | 1.77 | 0.89 | 4.4 | 14.2 | 0.95 | 2.5 | medium | SP | No |
| | A7 | 1.341 | 0.851 | 0.402 | 0.203 | 6.61 | 0.59 | 13.7 | 19.9 | 0.52 | 12.6 | coarse | SP | No |
| 10/8/2020 AM | A1 | 0.292 | 0.259 | 0.206 | 0.163 | 1.79 | 0.89 | 3.8 | 15.2 | 0.82 | 4.8 | medium | SP | No |
| | A4 | 0.279 | 0.250 | 0.200 | 0.161 | 1.73 | 0.90 | 3.5 | 14.5 | 0.90 | -0.2 | fine | SP | No |
| | A8 | 1.114 | 0.803 | 0.408 | 0.156 | 7.15 | 0.96 | 14.1 | 20.3 | 0.49 | 26.4 | coarse | SP | No |
| 10/8/2020 PM | A1 | 0.280 | 0.250 | 0.200 | 0.159 | 1.76 | 0.89 | 3.5 | 14.6 | 0.88 | 2.7 | medium | SP | No |
| | A3 | 0.275 | 0.246 | 0.196 | 0.156 | 1.76 | 0.89 | 2.7 | 15.0 | 0.82 | 2.6 | fine | SP | No |
| | A4 | 0.276 | 0.248 | 0.199 | 0.160 | 1.73 | 0.90 | 3.2 | 14.3 | 0.92 | 3.6 | fine | SP | No |
| 10/9/2020 AM | A1 | 0.315 | 0.277 | 0.215 | 0.167 | 1.89 | 0.88 | 0.7 | 15.2 | 0.76 | 0.8 | medium | SP | No |
| | A4 | 0.279 | 0.250 | 0.200 | 0.161 | 1.74 | 0.90 | 2.9 | 15.0 | 0.82 | 2.9 | fine | SP | No |
| | A7 | 0.685 | 0.459 | 0.283 | 0.182 | 3.76 | 0.64 | 8.3 | 16.4 | 0.76 | 10.1 | medium | SP | No |
| 10/9/2020 PM | A1 | 0.295 | 0.262 | 0.208 | 0.165 | 1.79 | 0.89 | 0.2 | 15.3 | 0.74 | 0.7 | medium | SP | No |
| | A4 | 0.278 | 0.250 | 0.201 | 0.162 | 1.72 | 0.90 | 2.1 | 14.6 | 0.86 | 2.5 | fine | SP | No |
| | A7 | 0.783 | 0.552 | 0.309 | 0.187 | 4.19 | 0.65 | 9.2 | 17.3 | 0.68 | 9.7 | coarse | SP | No |
| 11/9/2020 AM | A1 | 0.313 | 0.274 | 0.210 | 0.161 | 1.95 | 0.88 | 2.4 | 15.1 | 0.81 | 4.5 | medium | SP | No |
| | A4 | 0.370 | 0.317 | 0.232 | 0.170 | 2.18 | 0.86 | 10.4 | 13.9 | 1.11 | 10.9 | medium | SP | No |
| | A6 | 0.731 | 0.523 | 0.302 | 0.185 | 3.96 | 0.68 | 15.6 | 18.1 | 0.70 | 24.0 | coarse | SP | No |
| 11/10/2020 AM | A1 | 0.309 | 0.271 | 0.209 | 0.161 | 1.92 | 0.88 | 3.1 | 14.5 | 0.89 | 2.7 | medium | SP | No |
| | A4 | 0.527 | 0.423 | 0.275 | 0.178 | 2.95 | 0.80 | 7.0 | 15.7 | 0.81 | 14.7 | medium | SP | No |
| | A5 | 0.526 | 0.434 | 0.281 | 0.181 | 2.90 | 0.83 | 17.9 | 18.7 | 0.68 | 26.8 | medium | SP | No |
| | C5 | 0.967 | 0.718 | 0.341 | 0.192 | 5.04 | 0.63 | 4.9 | 15.9 | 0.75 | 8.1 | coarse | SP | No |
| 11/12/2020 PM | A1 | 0.284 | 0.251 | 0.197 | 0.154 | 1.84 | 0.89 | 8.5 | 16.4 | 0.76 | 11.8 | medium | SP | No |
| | A3 | 0.291 | 0.260 | 0.206 | 0.164 | 1.78 | 0.89 | 21.8 | 17.6 | 0.84 | 25.9 | medium | SP | No |
| 11/13/2020 AM | A1-1 | 0.272 | 0.242 | 0.191 | 0.151 | 1.80 | 0.89 | 11.6 | 20.9 | 0.42 | 17.1 | fine | SP | Yes |
| | A1-5 | 0.268 | 0.239 | 0.189 | 0.149 | 1.80 | 0.89 | 13.2 | 16.3 | 0.85 | 24.9 | fine | SP | Yes |
| | A1-12 | 0.291 | 0.259 | 0.205 | 0.163 | 1.79 | 0.89 | 9.9 | 24.4 | 0.20 | 18.9 | medium | SP | Yes |

| Date | Station | $d_{60}$ (mm) | $d_{50}$ (mm) | $d_{30}$ (mm) | $d_{10}$ (mm) | $C_u$ | $C_c$ | $w_c$ (%) | $\gamma$ (kN/m$^3$) | Void Ratio, $e$ | $M_v$ (%) | Wentworth Classification | USCS Classification | Heavy Minerals |
|---|---|---|---|---|---|---|---|---|---|---|---|---|---|---|
| 12/7/2020 AM | A1 | 0.298 | 0.263 | 0.205 | 0.159 | 1.87 | 0.88 | 5.2 | 15.6 | 0.79 | 4.7 | medium | SP | No |
| | A4 | 0.283 | 0.254 | 0.205 | 0.165 | 1.71 | 0.90 | 3.5 | 14.5 | 0.90 | 3.3 | medium | SP | No |
| | A7 | 0.349 | 0.302 | 0.226 | 0.169 | 2.06 | 0.87 | 12.2 | 15.9 | 0.88 | 22.5 | medium | SP | No |
| | B4 | 0.292 | 0.261 | 0.208 | 0.165 | 1.77 | 0.89 | 3.9 | 15.6 | 0.77 | 5.0 | medium | SP | No |
| 12/9/2020 AM | A1 | 0.269 | 0.240 | 0.190 | 0.151 | 1.79 | 0.89 | 5.2 | 16.1 | 0.74 | 5.8 | fine | SP | No |
| | A4 | 0.279 | 0.251 | 0.202 | 0.163 | 1.71 | 0.90 | 4.5 | 14.4 | 0.93 | 4.3 | medium | SP | No |
| | A6 | 0.302 | 0.268 | 0.211 | 0.166 | 1.81 | 0.89 | 19.1 | 17.9 | 0.77 | 29.4 | medium | SP | No |
| | B3 | 0.278 | 0.249 | 0.201 | 0.162 | 1.72 | 0.90 | 3.4 | 14.3 | 0.92 | 3.7 | fine | SP | No |
| 12/10/2020 PM | A1 | 0.291 | 0.257 | 0.201 | 0.158 | 1.84 | 0.88 | 3.7 | 15.3 | 0.80 | 4.2 | medium | SP | No |
| | A4 | 0.281 | 0.251 | 0.202 | 0.162 | 1.73 | 0.90 | 4.3 | 14.4 | 0.93 | 4.3 | medium | SP | No |
| | A7 | 0.296 | 0.263 | 0.209 | 0.166 | 1.79 | 0.89 | 15.2 | 16.6 | 0.84 | 15.8 | medium | SP | No |
| | C2 | 0.259 | 0.229 | 0.179 | 0.117 | 2.21 | 1.05 | 4.7 | 26.4 | 0.05 | 26.8 | fine | SP | Yes |
| 12/11/2020 PM | A1 | 0.295 | 0.261 | 0.205 | 0.160 | 1.84 | 0.88 | 2.7 | 15.1 | 0.81 | 3.9 | medium | SP | No |
| | A4 | 0.276 | 0.248 | 0.200 | 0.162 | 1.71 | 0.90 | 3.3 | 13.7 | 1.00 | 3.4 | fine | SP | No |
| | A7 | 0.318 | 0.280 | 0.217 | 0.168 | 1.90 | 0.88 | 10.9 | 15.3 | 0.93 | 10.7 | medium | SP | No |
| 1/20/2021 PM | 1 | 0.270 | 0.241 | 0.191 | 0.152 | 1.77 | 0.89 | 5.0 | 16.6 | 0.68 | 1.0 | fine | SP | No |
| | 3 | 0.246 | 0.215 | 0.165 | 0.101 | 2.44 | 1.09 | 4.3 | 17.6 | 0.58 | 16.2 | fine | SP | Yes |
| | 8 | 0.280 | 0.251 | 0.202 | 0.162 | 1.72 | 0.90 | 4.1 | 13.5 | 1.05 | 3.2 | medium | SP | No |
| 1/21/2021 AM | 23 | 0.251 | 0.219 | 0.168 | 0.103 | 2.43 | 1.09 | 4.3 | 18.1 | 0.53 | 12.4 | fine | SP | Yes |
| | 25 | 0.299 | 0.266 | 0.210 | 0.166 | 1.80 | 0.89 | 2.3 | 13.9 | 0.96 | 1.6 | medium | SP | No |
| | 26 | 0.308 | 0.273 | 0.214 | 0.167 | 1.84 | 0.89 | 5.0 | 14.4 | 0.94 | 4.4 | medium | SP | No |
| 4/20/2021 PM | A1 | 0.295 | 0.262 | 0.207 | 0.163 | 1.81 | 0.89 | 2.9 | 15.3 | 0.79 | 1.1 | medium | SP | No |
| | A4 | 0.340 | 0.296 | 0.225 | 0.171 | 1.99 | 0.87 | 2.4 | 14.6 | 0.86 | 1.9 | medium | SP | No |
| | A7 | 0.545 | 0.403 | 0.270 | 0.181 | 3.00 | 0.74 | 4.4 | 15.0 | 0.85 | 6.4 | medium | SP | No |
| | B10 | 1.149 | 0.967 | 0.664 | 0.446 | 2.57 | 0.86 | 17.4 | 16.4 | 0.90 | 29.9 | coarse | SP | No |
| 4/21/2021 AM | A1 | 0.283 | 0.251 | 0.197 | 0.154 | 1.84 | 0.89 | 1.2 | 15.8 | 0.70 | 1.0 | medium | SP | No |
| | A4 | 0.324 | 0.285 | 0.220 | 0.169 | 1.92 | 0.88 | 2.3 | 13.8 | 0.97 | 1.8 | medium | SP | No |
| | A7 | 0.318 | 0.281 | 0.218 | 0.169 | 1.89 | 0.88 | 4.8 | 14.4 | 0.93 | N/A | medium | SP | No |
| | C10 | 0.595 | 0.522 | 0.377 | 0.202 | 2.95 | 1.18 | 18.9 | 19.1 | 0.65 | N/A | coarse | SP | No |

| Date | Station | $d_{60}$ (mm) | $d_{50}$ (mm) | $d_{30}$ (mm) | $d_{10}$ (mm) | $C_u$ | $C_c$ | $w_c$ (%) | $\gamma$ (kN/m$^3$) | Void Ratio, $e$ | $M_v$ (%) | Wentworth Classification | USCS Classification | Heavy Minerals |
|---|---|---|---|---|---|---|---|---|---|---|---|---|---|---|
| | A1 | 0.287 | 0.257 | 0.206 | 0.165 | 1.74 | 0.89 | 1.3 | 15.5 | 0.74 | 0.3 | medium | SP | No |
| 4/22/2021 | A4 | 0.382 | 0.326 | 0.238 | 0.174 | 2.20 | 0.85 | 1.6 | 13.8 | 0.96 | 0.5 | medium | SP | No |
| AM | A7 | 0.351 | 0.304 | 0.228 | 0.171 | 2.05 | 0.87 | 5.5 | 14.9 | 0.88 | 11.4 | medium | SP | No |
| | B5 | 0.340 | 0.296 | 0.225 | 0.171 | 1.99 | 0.87 | 1.6 | 14.6 | 0.85 | 1.7 | medium | SP | No |
| | A1 | 0.270 | 0.241 | 0.191 | 0.152 | 1.77 | 0.89 | 1.0 | 15.6 | 0.72 | 0.5 | fine | SP | No |
| 4/22/2021 | A4 | 0.378 | 0.323 | 0.237 | 0.173 | 2.18 | 0.86 | 1.1 | 14.4 | 0.87 | 0.5 | medium | SP | No |
| PM | A7 | 0.362 | 0.312 | 0.232 | 0.172 | 2.10 | 0.86 | 2.8 | 14.4 | 0.90 | 3.1 | medium | SP | No |
| | C9 | 2.760 | 2.404 | 1.324 | 0.383 | 7.21 | 1.66 | 9.0 | 16.0 | 0.77 | 6.5 | very coarse | SW | No |
| | A1 | 0.286 | 0.256 | 0.206 | 0.165 | 1.73 | 0.90 | 0.5 | 15.7 | 0.70 | 0.6 | medium | SP | No |
| 4/23/2021 | A4 | 0.427 | 0.358 | 0.252 | 0.177 | 2.41 | 0.84 | 1.1 | 14.7 | 0.83 | 1.0 | medium | SP | No |
| AM | A7 | 0.340 | 0.296 | 0.225 | 0.171 | 1.99 | 0.87 | 3.1 | 14.8 | 0.85 | 2.6 | medium | SP | No |
| | C9 | 2.048 | 0.732 | 0.379 | 0.202 | 10.13 | 0.35 | 5.7 | 15.7 | 0.79 | 6.2 | coarse | SP | No |
| | A1 | 0.282 | 0.251 | 0.199 | 0.158 | 1.79 | 0.89 | 2.1 | 15.8 | 0.72 | 1.5 | medium | SP | No |
| 6/29/2021 | A4 | 0.292 | 0.260 | 0.207 | 0.164 | 1.78 | 0.89 | 1.4 | 14.6 | 0.85 | 0.9 | medium | SP | No |
| PM | A7 | 0.278 | 0.248 | 0.199 | 0.159 | 1.75 | 0.89 | 17.2 | 17.2 | 0.81 | 23.6 | fine | SP | No |
| | B9 | 0.309 | 0.272 | 0.211 | 0.163 | 1.89 | 0.88 | 18.2 | 19.6 | 0.60 | 35.7 | medium | SP | No |
| | A1 | 0.279 | 0.248 | 0.195 | 0.154 | 1.81 | 0.89 | 2.2 | 15.7 | 0.73 | 1.4 | fine | SP | No |
| 6/30/2021 | A4 | 0.285 | 0.255 | 0.204 | 0.163 | 1.74 | 0.89 | 1.4 | 14.3 | 0.88 | 0.8 | medium | SP | No |
| AM | A7 | 0.275 | 0.246 | 0.197 | 0.158 | 1.74 | 0.89 | 16.4 | 16.1 | 0.92 | 21.7 | fine | SP | No |
| | C10 | 0.342 | 0.296 | 0.222 | 0.167 | 2.05 | 0.87 | 22.6 | 19.1 | 0.71 | 34.7 | medium | SP | No |
| | A1 | 0.274 | 0.245 | 0.197 | 0.157 | 1.74 | 0.90 | 1.9 | 16.6 | 0.63 | 0.6 | fine | SP | No |
| 6/30/2021 | A4 | 0.288 | 0.257 | 0.205 | 0.164 | 1.76 | 0.89 | 0.9 | 15.1 | 0.78 | 0.5 | medium | SP | No |
| PM | A7 | 0.273 | 0.244 | 0.196 | 0.158 | 1.73 | 0.90 | 8.2 | 14.4 | 1.00 | 14.3 | fine | SP | No |
| | B8 | 0.367 | 0.311 | 0.222 | 0.159 | 2.31 | 0.85 | 16.7 | 19.7 | 0.57 | 33.6 | medium | SP | No |
| | A1 | 0.278 | 0.248 | 0.197 | 0.157 | 1.78 | 0.89 | 3.3 | 15.9 | 0.73 | 1.0 | fine | SP | No |
| 7/1/2021 | A4 | 0.300 | 0.267 | 0.210 | 0.166 | 1.81 | 0.89 | 1.0 | 14.5 | 0.85 | 16.9 | medium | SP | No |
| AM | A7 | 0.275 | 0.246 | 0.197 | 0.158 | 1.73 | 0.90 | 9.7 | 14.7 | 0.98 | 32.7 | fine | SP | No |
| | A10 | 0.302 | 0.266 | 0.206 | 0.160 | 1.89 | 0.88 | 21.3 | 19.7 | 0.64 | 0.7 | medium | SP | No |

| Date | Station | $d_{60}$ (mm) | $d_{50}$ (mm) | $d_{30}$ (mm) | $d_{10}$ (mm) | $C_u$ | $C_c$ | $w_c$ (%) | γ (kN/m$^3$) | Void Ratio, $e$ | $M_v$ (%) | Wentworth Classification | USCS Classification | Heavy Minerals |
|---|---|---|---|---|---|---|---|---|---|---|---|---|---|---|
| 10/13/2021 Noon | CRAB 1 | 0.509 | 0.405 | 0.270 | 0.179 | 2.84 | 0.80 | 19.4 | 20.0 | 0.552 | 21.6 | medium | SP | No |
| | CRAB 2 | 0.353 | 0.305 | 0.227 | 0.169 | 2.09 | 0.86 | 14.5 | 16.8 | 0.772 | 20.6 | medium | SP | No |
| | CRAB 3 | 0.308 | 0.272 | 0.212 | 0.165 | 1.87 | 0.88 | 5.5 | 15.4 | 0.78 | 6.3 | medium | SP | No |
| | CRAB 4 | 0.446 | 0.372 | 0.257 | 0.178 | 2.51 | 0.83 | 11.2 | 16.2 | 0.78 | 11.2 | medium | SP | No |
| | CRAB 7 | 0.445 | 0.371 | 0.257 | 0.178 | 2.50 | 0.83 | 20.9 | N/A | | 20.9 | medium | SP | No |
| | CRAB 13 | 0.343 | 0.298 | 0.225 | 0.170 | 2.02 | 0.87 | 21.7 | N/A | | 21.7 | medium | SP | No |
| | CRAB 16 | 0.282 | 0.249 | 0.193 | 0.150 | 1.88 | 0.88 | 4.6 | N/A | | 4.6 | fine | SP | No |
| 10/13/2021 PM | A1 | 0.311 | 0.271 | 0.206 | 0.156 | 1.99 | 0.87 | 3.1 | N/A | | 3.4 | medium | SP | No |
| | A4 | 0.316 | 0.279 | 0.216 | 0.168 | 1.89 | 0.88 | 5.2 | 15.0 | 0.826 | 4.2 | medium | SP | No |
| | A7 | 0.517 | 0.441 | 0.289 | 0.185 | 2.79 | 0.87 | 20.1 | 20.7 | 0.512 | 31.2 | medium | SP | No |
| | B7 | 1.159 | 0.848 | 0.441 | 0.211 | 5.49 | 0.80 | 12.9 | N/A | | 24.8 | coarse | SP | No |
| | C1 | 0.273 | 0.243 | 0.192 | 0.152 | 1.80 | 0.89 | 5.7 | N/A | | 1.7 | fine | SP | No |
| | C5 | 0.301 | 0.267 | 0.210 | 0.165 | 1.82 | 0.89 | 5.7 | N/A | | 7.2 | medium | SP | No |
| | C7 | 0.382 | 0.325 | 0.236 | 0.172 | 2.22 | 0.85 | 16.2 | N/A | | 20.6 | medium | SP | No |
| | D5 | 0.317 | 0.278 | 0.215 | 0.166 | 1.91 | 0.88 | 11.3 | N/A | | 7.8 | medium | SP | No |

**References**


ASTM. 2014. “Standard Test Method for Electronic Friction Cone and Piezocone Penetration Testing.” i: 1–21. https://doi.org/10.1520/D5778-20.2.

De Beer, E. E. 1970. “Experimental determination of the shape factors and the bearing capacity factors of sand.” *Geotechnique*, 20 (4): 387–411. https://doi.org/10.1680/geot.1970.20.4.387.

Brodie, K. L., T. Dyer, N. Spore, R. Slocum, A. O’Dea, T. Whitesides, and R. Alexander. 2017. “Continuously Operating Dune-Mounted Lidar System at the Field Research Facility, A Report Detailing Lidar Collection, Processing, Evaluation, and Product Development.”

Famiglietti, J. S., J. W. Rudnicki, and M. Rodell. 1998. “Variability in surface moisture content along a hillslope transect: Rattlesnake Hill, Texas.” *Journal of Hydrology*, 210 (1–4): 259–281. Elsevier. https://doi.org/10.1016/S0022-1694(98)00187-5.

Kuester, M. 2016. “Radiometric Use of WorldView-3 Imagery.” *Technical Note*, 12.

Lucking, G., N. Stark, T. Lippmann, and S. Smyth. 2017. “Variability of in situ sediment strength and pore pressure behavior of tidal estuary surface sediments.” *Geo-Marine Letters*, 37 (5): 441–456. Geo-Marine Letters. https://doi.org/10.1007/s00367-017-0494-6.

Meyerhof, G. G. 1963. “Some Recent Research on the Bearing Capacity of Foundations.” *Canadian Geotechnical Journal*, 1 (1): 16–26. https://doi.org/10.1139/t63-003.

Muller, E., and H. Décamps. 2001. “Modeling soil moisture - Reflectance.” *Remote Sensing of Environment*, 76 (2): 173–180. https://doi.org/10.1016/S0034-4257(00)00198-X.

Oh, Y. 2004. “Quantitative retrieval of soil moisture content and surface roughness from multipolarized radar observations of bare soil surfaces.” *IEEE Transactions on Geoscience and Remote Sensing*, 42 (3): 596–601. https://doi.org/10.1109/TGRS.2003.821065.

Paprocki, J. 2022a. “A Framework for Assessing Lower-Bound Bearing Capacity of Sandy Coastal Sediments from Remotely Sensed Imagery.” Virginia Tech.

Paprocki, J. 2022b. “Data Associated with A Framework for Assessing Lower-Bound Bearing Capacity of Sandy Coastal Sediments from Remotely Sensed Imagery.” *University Libraries, Virginia Tech*.

Paprocki, J., N. Stark, H. C. Graber, H. Wadman, and J. E. McNinch. 2022. “Assessment of moisture content in sandy beach environments from multispectral satellite imagery.” *Canadian Geotechnical Journal*, 59 (2): 225–238. https://doi.org/10.1139/cgj-2020-0624.

Stark, N., A. E. Hay, and G. Trowse. 2014. “Cost-effective geotechnical and sedimentological early site assessment for ocean renewable energies.” *2014 Oceans - St. John’s*, 1–8. IEEE.

Stark, N., A. Kopf, H. Hanff, S. Stegmann, and R. Wilkens. 2009. “Geotechnical investigations of sandy seafloors using dynamic penetrometers.” *OCEANS 2009*, 1–10. IEEE.

Stark, N., B. Radosavljevic, B. Quinn, and H. Lantuit. 2017. “Application of portable free-fall penetrometer for geotechnical investigation of arctic nearshore zone.” *Canadian Geotechnical Journal*, 54 (1): 31–46. https://doi.org/10.1139/cgj-2016-0087.

Stark, N., R. Wilkens, V. B. Ernstsen, M. Lambers-Huesmann, S. Stegmann, and A. Kopf. 2012. “Geotechnical Properties of Sandy Seafloors and the Consequences for Dynamic Penetrometer Interpretations: Quartz Sand Versus Carbonate Sand.” *Geotechnical and Geological Engineering*, 30 (1): 1–14. https://doi.org/10.1007/s10706-011-9444-7.

Stephan, S., N. Kaul, and H. Villinger. 2015. “Validation of impact penetrometer data by cone penetration testing and shallow seismic data within the regional geology of the Southern North Sea.” *Geo-Marine Letters*, 35 (3): 203–219. https://doi.org/10.1007/s00367-015-0401-y.

Stoll, R. D., Y. F. Sun, and I. Bitte. 2007. “Seafloor properties from penetrometer tests.” *IEEE Journal of Oceanic Engineering*, 32 (1): 57–63. https://doi.org/10.1109/JOE.2007.890943.

Vesić, A. S. 1973. “Analysis of Ultimate Loads of Shallow Foundations.” *ASCE J Soil Mech Found Div*.